Inertial Effects on Flow and Transport in Heterogeneous Porous Media

Alon Nissan[*] and Brian Berkowitz

Department of Earth and Planetary Sciences, Weizmann Institute of Science, Rehovot 7610001, Israel

We investigate the effects of high fluid velocities on flow and tracer transport in heterogeneous porous media. We simulate fluid flow and advective transport through two-dimensional pore-scale matrices with varying structural complexity. As the Reynolds number increases, the flow regime transitions from linear to nonlinear; this behavior is controlled by the medium structure, where higher complexity amplifies inertial effects. The result is, nonintuitively, increased homogenization of the flow field, which leads in the context of conservative chemical transport to less anomalous behavior. We quantify the transport patterns via a continuous time random walk, using the spatial distribution of the kinetic energy within the fluid as a characteristic measure.

Natural geological formations are characterized by a complex, irregular, heterogeneous spatial structure that strongly affects the dynamics of fluid flow and chemical transport [1]. This heterogeneity leads to non-Gaussian, multiscale velocity field distributions [2], which in the context of transport induces non-Fickian (anomalous) behavior [3].

Single-phase flow in porous media is usually described by Darcy's law, $\mathbf{V} = -(\mathbf{k}/\mu)\nabla I$, where μ is the fluid dynamic viscosity and the permeability tensor of the domain, $\mathbf{k}$, controls the average fluid velocity $\mathbf{V}$ under an external pressure gradient ∇I. This expression follows directly from the Navier-Stokes equations by assuming that the inertial effects and terms that express energy dissipation can be neglected as a result of momentum transfer within the fluid [4]. This is generally a good approximation for viscous flow conditions (low Reynolds numbers). However, in natural geological formations, where structural heterogeneity exists at every scale—from continuous, pore-scale heterogeneity fluctuations through abrupt heterogeneity changes between different geological units—these assumptions may be seriously misleading.

Andrade *et al.* [5] examined the contribution of inertia to flow, in terms of stream functions, in two-dimensional domains with randomly distributed obstacles. In these sparse domains, with a porosity of 0.9, they found that viscous forces generate well-defined preferential channels for fluid flow at low Reynolds numbers (Re). In contrast, this channeling effect is less intense for higher Re, and due to the relative contribution of inertial forces, the streamline distribution in the direction orthogonal to the main flow becomes more spatially homogeneous. It is unclear, however, how inertial effects impact these flow phenomena [6] and chemical transport [7] in heterogeneous geological porous media, where porosities are significantly lower and the pore space configuration is highly irregular.

Chemical transport in heterogeneous porous media is determined by the interplay between advection and diffusion. For advection-dominated regimes, where molecular diffusion can be neglected, the transport of chemicals essentially follows the velocity field streamlines. Therefore, correct interpretation of the velocity field spatial distribution is a key aspect in predicting chemical transport in porous media [8–10]. In this context, the preferential flow paths induced by structural heterogeneity lead to focusing of chemical transport [11,12]; hence, only a portion of the velocity field controls most of the transport. Flekkøy *et al.* [13] studied the effects of inertia on tracer movement in Hele-Shaw cells with a single obstacle. They found the even at relatively low Re (Re ≥ 0.02) the irreversibility observed in forward-backward (echo) flow experiments is due to inertial forces, in addition to molecular diffusion.

The purpose of this Letter is to demonstrate the effect of Re on fluid flow and transport of conservative (nonreactive) chemical species through porous media with various patterns of structural heterogeneity. In particular, we show how the regions in the domain that actively participate in the transport, and the range of velocity values that are sampled during the transport, vary under different flow regimes as a result of inertial effects. We then interpret the resulting transport behavior within the continuous time random walk (CTRW) framework, using the spatial distribution of the kinetic energy within the fluid—which is itself a function of Re—as a characteristic measure.

We generated three types of two-dimensional, heterogeneous porous media systems, each with an average porosity of 0.45. The porous systems are based on a pore-scale image adapted from a natural rock material [14], with a porosity of 0.58, which was rendered as a black and white image of solid grains and pore space, respectively. This image formed the basic template (unit) for the

porous media we consider; this unit was then modified twice by scaling (enlarging) the solid phase uniformly around the perimeter of each solid grain, to obtain three topologically similar porous units with porosities of 0.32, 0.45, and 0.58. Each of the three heterogeneous systems was constructed randomly from these pore-scale units; we generated 10 realizations of each system, with overall dimensions of 8 cm (width) ×6 cm (height). The porous media systems (Fig. 1) are characterized here as the homogeneous system (HS), randomly heterogeneous system (RHS), and structured heterogeneity system (SHS). The HS and SHS are composed of (4×3) 12 units, while the RHS contains (16×12) 192 units. Below, we refer to the order HS, RHS, SHS as an increase in heterogeneity.

Fluid flow through these systems (Fig. 1) was determined by solving (using COMSOL Multiphysics®) the Navier-Stokes equations for steady, incompressible flow: $\rho(\mathbf{U} \cdot \boldsymbol{\nabla}\mathbf{U}) = -\boldsymbol{\nabla}p + \mu\boldsymbol{\nabla}^2\mathbf{U}; \; \boldsymbol{\nabla} \cdot \mathbf{U} = 0$, where $\mathbf{U}$ is the pore-scale (local) fluid velocity, p is the fluid pressure, and ρ is the fluid density. No-slip conditions are applied at the fluid-solid interface. A constant velocity is specified in the normal direction to the inlet boundary (left side), and a constant reference pressure is prescribed at the outlet (right side). The remaining (horizontal) boundaries are treated as impermeable. These conditions are representative of many experimental setups for macroscopically one-dimensional flow and transport [15,16]. The Re in the simulations is defined as Re= $\rho d_p \bar{U}/\mu$, where $\bar{U}$ is the average fluid velocity and d_p is the average diameter (1 mm) of the solid particles. The range of Re values considered here was $10^{-4} < $ Re $ < 10^1$, within the laminar flow regime [5,17]. Note that streamlines resulting from solution of the Navier-Stokes equations are determined by both the value of Re and the presence and configuration of the solid grains ("obstacles"), which lead to expansion and compression of streamlines in the vicinity of the solid grains.

To evaluate inertial effects on conservative chemical transport, we consider advection-dominated regimes, and

neglect molecular diffusion to avoid effects that arise from the interplay between advection and diffusion. We point out that, as shown below, effects of inertia become significant at higher Re—i.e., for higher average fluid velocities across the domain—so that the influence of diffusion can generally be neglected given the different time scales between advection and diffusion. Chemical transport is modeled by a particle tracking algorithm (with 10^5 particles representing chemical mass) that uses a semianalytic streamline-based method [9] to simulate particle movement by advection along the velocity-field streamlines. Particles are introduced to the system by a pulse injection, with a flux-weighted distribution along the inlet boundary, and monitored until they exit from the outlet boundary.

To assess changes in the spatial distribution of the flow field that result from increasing the effect of inertial forces, we quantify the statistics of the flow-field kinetic energy distribution. We divide the flow domain into a grid containing $n = 3000 \times 2000$ (x, y axes) cells. Following Andrade *et al.* [5], we define a "participation" number π as

$$\pi \equiv \left(n \sum_{i=1}^{n} q_i^2 \right)^{-1}, \qquad (1)$$

where $q_i \equiv e_i / \sum_{j=1}^{n} e_j^2$, $e_i \propto (u_i^2 + v_i^2)$ is the kinetic energy of the fluid cells, and u_i and v_i are the velocity components of $\mathbf{U}$. From Eq. (1), the participation number range is $0 \le \pi \le 1$; $\pi = 1$ for a purely homogeneous system, whereas the velocity field shows strongly defined (spatial) preferential paths when $\pi \to 0$.

Figure 2 shows π as a function of Re in the three porous media systems (HS, RHS, and SHS). The large increase in
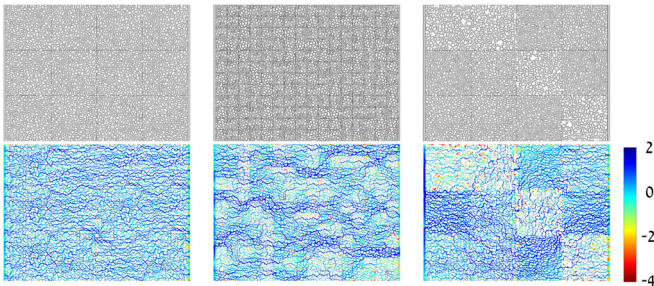

FIG. 1. Spatial structure (top row) and normalized velocity field (bottom row) for the different systems (from left to right): homogeneous system (HS), randomly heterogeneous system (RHS), and structured heterogeneous system (SHS). HS and SHS are each composed of (4×3) 12 units, and the RHS contains (16×12) 192 units. The color bar is in logarithmic scale $\log(\mathbf{U}/\bar{U})$.
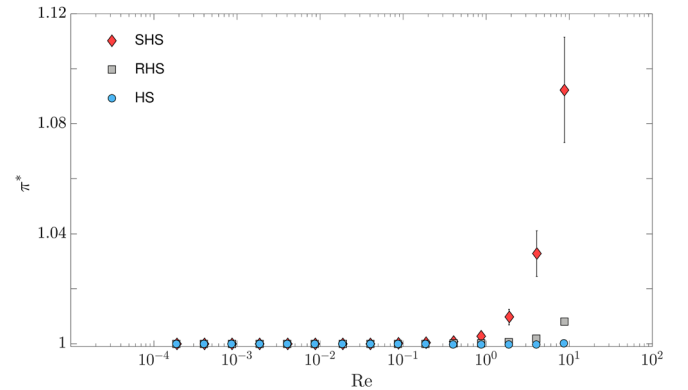

FIG. 2. Dependence of the normalized participation number (π^*) on Reynolds number (Re), for HS (blue circles), RHS (gray squares), and SHS (red diamonds), averages of 10 realizations for each system. In each case, π was normalized by the initial value (at the smallest Re), so that the first value is equal to 1; thus, while $0 \le \pi \le 1$, here $\pi^* \ge 1$. Because the spatial distribution of the velocity field may vary significantly among realizations, particularly for the SHS, we use π^* to examine the standard deviation of the realizations (error bars). Where not visible, the error bars lie within the symbols.

π at a specific Reynolds, $Re^* \approx 1$, indicates the transition between the linear (Darcy's law) regime and nonlinear behavior; the transition occurs at smaller Re^* as the medium heterogeneity increases.

We find that for all systems (and for each of the individual realizations), π depends on Re as $\pi = \pi_0 + \zeta Re^\lambda$ (so that $\pi^* = 1 + \zeta^* Re^\lambda$), where ζ and λ relate to contributions of inertia. The numerical simulations clearly demonstrate that the effect of inertia depends on structural heterogeneity of the medium; from analysis of the simulations, we have that ζ increases with heterogeneity ($\zeta_{HS} = 1.7 \times 10^{-8}$, $\zeta_{RHS} = 3.36 \times 10^{-5}$, $\zeta_{SHS} = 3.31 \times 10^{-4}$), and λ decreases ($\lambda_{HS} = 3.6$, $\lambda_{RHS} = 1.88$, $\lambda_{SHS} = 1.45$). The initial flow field homogeneity index, π_0, decreases with heterogeneity ($\pi_0 = 0.24, 0.17$ and 0.11, for HS, RHS, and SHS, respectively).

We now examine conservative chemical transport in these systems. For purely advective transport, chemical species ("particles") simply follow the streamlines. However, due to the role of preferential paths and stagnant (low velocity) zones within the flow field, migrating chemicals do not fully sample the spatial domain nor the range of velocity values in the velocity field distribution [12]. We analyze the effect of Re on the portion of the velocity field that actually contributes to the transport. In each realization, we record the grid cells that are visited by particles throughout the simulation. This information was collected for different Re, with 10 realizations for each porous medium system. The particle visitation maps were transformed using the stationary velocity field into a probability density function of normalized velocities $\Omega = PDF(U_p/\bar{U})$, where $\bar{U}$ is the average velocity and U_p is the local particle velocity in each cell.

Figure 3 (left column) shows Ω for each system, with two Re that are in the vicinity of the transition zone (Re^*) of π. Similar to the results depicted in Fig. 2, the inertial effects become evident as the structural heterogeneity increases, and result in a faster decline over the lower range of $U_p/\bar{U}$. Thus as Re increases, the velocity field distribution controlling chemical transport becomes narrower, thus leading to more uniform transport and reducing the degree of anomalous behavior. The right column in Fig. 3 indicates the slope $(1 + \beta)$ of the power-law region ($U_p/\bar{U} < 1$) in Ω, for each Re, averaged over 10 realizations. Similar to π (Fig. 2), we find a transition zone with a power dependency (solid lines).

The inset (Fig. 3) compares the velocity field distribution of the fluid throughout the system and the distribution of velocities experienced by the migrating chemical species, for a single realization. Clearly, the particle distribution differs from the fluid velocity field distribution, with higher velocity grid cells being sampled more heavily. Thus, to predict transport behavior in porous media, one must consider the velocity distribution actually sampled by chemical species, rather than the overall flow field
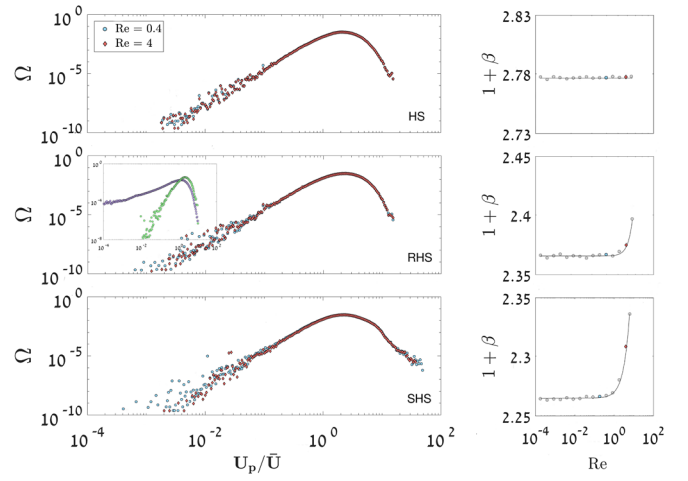

FIG. 3. Left column: Probability density function (Ω) of the normalized particle velocities ($U_p/\bar{U}$), averaged over 10 realizations, for Re = 0.4 (blue) and Re = 4 (red); HS (upper), RHS (middle), and SHS (bottom). Right column: The slope $(1 + \beta)$ of the Ω power-law region for each Re (each averaged over 10 realizations). The two colored markers in the plots represent the Re shown in the left column. Inset: Comparison between the velocity field density functions (for a single realization) of the fluid throughout the system (purple) and the particles that are transported within it (green) with Re = 0.4.

distribution. We point out, too, that increasing Re was found (not shown) to have a functionally negligible effect on the difference in velocity distributions, such as those appearing in the inset of Fig. 3—affecting only a small portion of the tail of lowest fluid velocities—relative to the effect of changing Re on the particle velocity distributions. Note that increasing the number of particles by an order of magnitude yielded the same results in all cases.

To quantify the impact of Re on the transport of chemical species, we use the CTRW framework [3,18], which treats tracer motion in porous media as particles undergoing various types of transitions. These transitions are defined by $\psi(t) dt$, which is the probability of a particle that just arrived at a site moving to an adjacent site in a time between t and $t + dt$. Because the distance between successive cells is constant, the particle transition in space has a narrow range, and $\psi(t)$ is directly proportional to $1/\Omega$ [9,12]. The long time tailing of $\psi(t)$ (i.e., the low velocity zone of Ω) is the feature that determines the transport propagation [3], and it is the region most affected by the magnitude of Re (Fig. 3). This part of $\psi(t)$ can be approximated by a power-law dependence $\psi(t) \sim t^{-1-\beta}$ [19], where β ($0 < \beta < 2$) takes into account the velocity field distribution that controls transport, and higher values of β (less anomalous transport behavior) are compatible with more homogeneous flow fields. Because $\psi(t) \propto 1/\Omega \sim t^{-1-\beta}$, we can evaluate β from the results in Fig. 3 (right column). Thus $\psi(t)$, like π, is modified according to Re. Inertial effects cause a similar change in the spatial distribution of

the kinetic energy within the fluid (π), and in the power-law region of the particle velocity distribution ($1 + \beta$), so that we find the power dependency of $(1 + \beta)^*$, i.e., $1 + \beta$ normalized by its initial value, to be similar to π^* (with $\leq 3\%$ deviation). Thus, $(1 + \beta)^* \approx \pi^* = 1 + \zeta^* \text{Re}^\lambda$, so that $1 + \beta \propto \pi$.

As a result, we expect that higher Re (Re $\geq$ Re*) will reduce the degree of anomalous transport behavior (β increases). This can be quantified by analyzing the particle breakthrough curves (BTCs) obtained from the streamline-based particle tracking simulations. Figure 4 shows the normalized cumulative BTCs ($\mathcal{N}_p$) for the three systems (each with a representative realization of the system), at different Re (near Re*). For comparison, the time axis (τ) was normalized between $0 \leq \tau \leq 1$, by the final times of the simulations (which are proportional to the fluid average velocity, $\bar{U}$). In addition, we used the CTRW framework in a particle tracking approach (solid and dashed lines), using a truncated power law function for $\psi(t)$ (see Ref. [20] for more information about the CTRW particle tracking method). Values of β used in the simulations were prescribed using the slope of the particle velocity distribution, $1 + \beta$ (Fig. 3, right column), at each Re (HS, $\beta_{\text{Re}=0.4} \approx \beta_{\text{Re}=4} = 1.78$; RHS, $\beta_{\text{Re}=0.4} = 1.36$ and $\beta_{\text{Re}=4} = 1.37$; SHS, $\beta_{\text{Re}=0.4} = 1.26$ and $\beta_{\text{Re}=4} = 1.31$), with increases in β over increasing Re of 0.02%, 0.8%, and 3.9% for HS, RHS, and SHS, respectively. These percentage increases are similar (not shown) to the relative increases in π^* with increasing Re (Fig. 2). While these increases might be considered small, they have a significant impact on the degree of anomalous tracer transport (see Fig 4).

To conclude, we confirm that deviation from a linear flow (Darcy's law) regime occurs as Re increases, and intensifies when the spatial heterogeneity of the porous medium increases. The structural heterogeneity is manifested both in terms of pore-scale variability and the existence of larger-scale, abrupt structural variations. Thus, when these variations are coupled to relatively high fluid velocities (but still within the laminar flow regime),
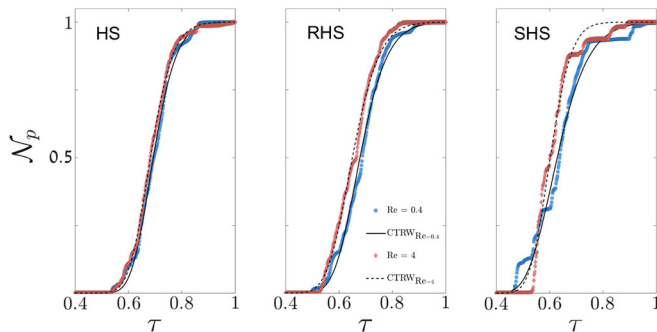
the contribution of inertia to fluid flow and chemical transport is amplified. Somewhat nonintuitively, however, we demonstrate that the fluid velocity field tends to become more spatially homogeneous with an increase in Re; the sensitivity to the transition and the strength of the nonlinear behavior are controlled by the structure of the medium. We emphasize that these findings are generic, in the sense that they can be expected to be valid for any heterogeneous porous medium with similar boundary conditions. We quantified this behavior via the participation number π; we find that $\pi = \pi_0 + \zeta \text{Re}^\lambda$, where ζ and λ represent system-dependent contributions to inertia, and π_0 characterizes the Darcy regime.

We also showed that the distribution of particle velocities deviates strongly from the velocity field distribution in the entire domain (Fig. 3, inset); particles tend to follow high velocity regions, and avoid the low velocity regions (preferential pathways), as a function of medium structure but also as a function of Re. This behavior is of immense importance when attempting to predict transport behavior through direct interpolation of the fluid velocity field, as done in many frameworks. We note that in cases where relevant, the impact of molecular diffusion is expected to reduce some of the impact of preferential paths on flow and transport. We also suggest that the dominance of preferential flow paths will increase in three-dimensional systems, so that the effect of inertia on advective-dominated transport can be expected to be at least as strong as in the two-dimensional systems considered here.

Significantly, with increasing Re, the portion of the velocity field that actively contributes to chemical advection-dominated transport exhibits increasingly narrower distributions of velocity values. This result leads to more uniform chemical transport, reducing the degree of anomalous behavior. This behavior was quantified by determining particle breakthrough curves (Fig. 4), and deriving the particle Lagrangian-velocity distribution (Fig. 3), to interpret the effects of high velocities on transport within the CTRW framework. The CTRW matches the BTCs (Fig. 4) by using β derived from the particle velocity distribution (Fig. 3). This leads us to use the spatial distribution of the kinetic energy within the fluid—which is itself a function of Re—as a characteristic measure that determines $1 + \beta \propto \pi$ for transport in porous materials in the presence of inertia.

The range of Re numbers examined here, wherein effects of inertia are shown to be significant—Re $\sim$0.1–10—is relevant in laboratory systems and in natural subsurface geological environments, in cases where flow rates are relatively high. For the latter, this is particularly relevant in the vicinity of pumping and injection wells (which are often used for domain characterization via tracer testing), and in fractured porous systems where velocities in fractures can be significantly higher than in porous media. In this context too, with an increasingly homogeneous flow field with increasing Re, an effect of inertia is to reduce the degree of

FIG. 4. Normalized cumulative breakthrough curves ($\mathcal{N}_p$) for two Re, using the streamline-based particle tracking simulations (markers) and the associated CTRW framework results (lines), Re = 0.4 (blue), and Re = 4 (red).

spreading and mixing for any given heterogeneous porous domain. This, in turn, affects not only conservative chemical transport, but can also be expected to influence the dynamics of reactive chemical transport and associated reaction rates. Given that inertia is seen to strongly impact fluid flow and chemical transport in natural porous media—even at Re $<$ 1—the findings here have major significance for understanding and quantification of these phenomena in geological environments.

––––––––––––

[*]alon.nissan@weizmann.ac.il

[1] G. Dagan, *Flow and Transport in Porous Formations* (Springer, Berlin, Heidelberg, 1989), pp. xvii and 465.

[2] B. Bijeljic, A. Raeini, P. Mostaghimi, and M. J. Blunt, Phys. Rev. E **87**, 013011 (2013).

[3] B. Berkowitz, A. Cortis, M. Dentz, and H. Scher, Rev. Geophys. **44**, RG2003 (2006).

[4] J. Bear, *Dynamics of Fluids in Porous Media* (American Elsevier Publishing Company, New York, 1972), p. 764.

[5] J. S. Andrade, U. M. S. Costa, M. P. Almeida, H. A. Makse, and H. E. Stanley, Phys. Rev. Lett. **82**, 5249 (1999).

[6] D. Lasseux and F. J. Valds-Parada, C.R. Mec. **345**, 660 (2017).

[7] N. Sund, D. Bolster, S. Mattis, and C. Dawson, Transp. Porous Media **109**, 411 (2015).

[8] B. Berkowitz and H. Scher, Phys. Rev. Lett. **79**, 4038 (1997).

[9] B. Bijeljic, P. Mostaghimis, and M. J. Blunt, Phys. Rev. Lett. **107**, 204502 (2011).

[10] T. Le Borgne, M. Dentz, and J. Carrera, Phys. Rev. Lett. **101**, 090601 (2008).

[11] M. Bianchi, C. Zheng, C. Wilson, G. R. Tick, G. Liu, and S. M. Gorelick, Water Resour. Res. **47** (2011).

[12] Y. Edery, A. Guadagnini, H. Scher, and B. Berkowitz, Water Resour. Res. **50**, 1490 (2014).

[13] E. G. Flekkøy, T. Rage, U. Oxaal, and J. Feder, Phys. Rev. Lett. **77**, 4170 (1996).

[14] R. Seright and F. Martin, New Mexico Institute for Mining and Technology/New Mexico Petroleum Recovery Research Center, Report No. DOE/BC/14447-15, DOE contract number FG22-89BC14447, 1992.

[15] S. E. Silliman, Water Resour. Res. **37**, 1883 (2001).

[16] B. Berkowitz and H. Scher, Adv. Water Resour. **32**, 750 (2009).

[17] B. P. Muljadi, M. J. Blunt, A. Q. Raeini, and B. Bijeljic, Adv. Water Resour. **95**, 329 (2016).

[18] E. W. Montroll and H. Scher, J. Stat. Phys. **9**, 101 (1973).

[19] M. Dentz, A. Cortis, H. Scher, and B. Berkowitz, Adv. Water Resour. **27**, 155 (2004).

[20] A. Nissan, I. Dror, and B. Berkowitz, Water Resour. Res. **53**, 3760 (2017).